THE JOURNAL OF BIOLOGICAL CHEMISTRY VOL. 288, NO. 24, pp. 17134–17144, June 14, 2013

Erythrocytosis and Pulmonary Hypertension in a Mouse Model of Human *HIF2A* Gain of Function Mutation*

Received for publication, December 11, 2012, and in revised form, April 25, 2013 Published, JBC Papers in Press, May 2, 2013, DOI 10.1074/jbc.M112.444059

Qiulin Tan[‡], Heddy Kerestes[‡], Melanie J. Percy[§], Ralph Pietrofesa[¶], Li Chen[‖], Tejvir S. Khurana[**], Melpo Christofidou-Solomidou[¶], Terence R. J. Lappin[‡‡], and Frank S. Lee[‡1]

*From the [‡]Department of Pathology and Laboratory Medicine, Divisions of [¶]Pulmonary, Allergy and Critical Care, and [‖]Cardiovascular Medicine, Department of Medicine, and **Department of Physiology and Pennsylvania Muscle Institute, Perelman School of Medicine, University of Pennsylvania, Philadelphia, Pennsylvania 19104, the [§]Department of Haematology, Belfast City Hospital, Belfast, Northern Ireland BT9 7AB, United Kingdom , and the [‡‡]Centre for Cancer Research and Cell Biology, Queen's University, Belfast, Northern Ireland BT9 7BL, United Kingdom*

Background: Missense mutations have been identified in the *HIF2A* gene in patients with erythrocytosis.
Results: A mouse knock-in line that models the first described *HIF2A* mutation exhibits erythrocytosis and pulmonary hypertension.
Conclusion: The missense mutation is the cause of erythrocytosis, and is accompanied by pulmonary hypertension.
Significance: The study demonstrates sequelae of global Hif-2α gain of function.

The central pathway for oxygen-dependent control of red cell mass is the prolyl hydroxylase domain protein (PHD):hypoxia inducible factor (HIF) pathway. PHD site specifically prolyl hydroxylates the transcription factor HIF-α, thereby targeting the latter for degradation. Under hypoxia, this modification is attenuated, allowing stabilized HIF-α to activate target genes, including that for erythropoietin (EPO). Studies employing genetically modified mice point to Hif-2α, one of two main Hif-α isoforms, as being the critical regulator of Epo in the adult mouse. More recently, erythrocytosis patients with heterozygous point mutations in the *HIF2A* gene have been identified; whether these mutations were polymorphisms unrelated to the phenotype could not be ruled out. In the present report, we characterize a mouse line bearing a G536W missense mutation in the *Hif2a* gene that corresponds to the first such human mutation identified (G537W). We obtained mice bearing both heterozygous and homozygous mutations at this locus. We find that these mice display, in a mutation dose-dependent manner, erythrocytosis and pulmonary hypertension with a high degree of penetrance. These findings firmly establish missense mutations in HIF-2α as a cause of erythrocytosis, highlight the importance of this HIF-α isoform in erythropoiesis, and point to physiologic consequences of HIF-2α dysregulation.

Red cell mass is highly responsive to changes in and inversely related to oxygen concentration. The central pathway by which changes in oxygen concentration are transduced to changes in red cell mass is the prolyl hydroxylase domain protein (PHD)[2]:hypoxia inducible factor (HIF) pathway (1–3). In this pathway, PHD prolyl hydroxylates HIF-α in an oxygen-dependent manner (4–6). There are three PHD isoforms, PHD1, PHD2, and PHD3, and there are two main HIF-α isoforms, HIF-1α and HIF-2α. The primary site of prolyl hydroxylation is Pro-564 in HIF-1α and Pro-531 in HIF-2α. This distinctive post-translational modification allows the binding of the von Hippel Lindau protein (VHL). VHL is a component of an E3 ubiquitin ligase that targets hydroxylated HIF-α for degradation by the proteasome. Under hypoxic conditions, this modification is arrested, allowing the stabilization of HIF-α and activation of HIF target genes.

The prototypical HIF target gene is the *EPO* gene (3, 7). Low tissue oxygenation results in activation of the HIF pathway and increased *EPO* transcription, leading to increased circulating levels of EPO. EPO then binds to the EPO receptor (EPOR) on erythroid precursors, resulting in expansion of red cell mass and producing an increase in the oxygen carrying capacity of the blood. The kidney is the primary organ source of EPO in adults, although the liver, brain, and bone are other potential sources (8–10).

Erythrocytosis is an uncommon condition characterized by abnormally high red cell mass, and it has provided an opportunity to gain insight into the oxygen-sensing pathway in humans (2). The first mutation identified in this pathway was the Chuvash mutation in the *VHL* gene (R200W) (11). This hypomorphic mutation leads to an impaired ability of VHL to degrade hydroxylated HIF-α. The second mutation identified in this pathway was a missense mutation in the *PHD2* gene (12). Subsequent studies in mice have demonstrated a central role for *Phd2* in erythropoiesis (13, 14).

The particular isoform of HIF-α regulating EPO has been a topic of substantial investigation. In mouse embryo and yolk

* This work was supported, in whole or in part, by National Institutes of Health Grants R01-CA153347 (to F. S. L.) and P30-DK19525 (to the Penn Diabetes Endocrine Research Center).
This work is dedicated to the memory of Dr. Yulan Sun.
[1] To whom correspondence should be addressed: Perelman School of Medicine, University of Pennsylvania, 605 Stellar Chance Labs, 422 Curie Blvd., Philadelphia, PA 19104. Tel.: 215-898-4701; Fax: 215-573-2272; E-mail: franklee@mail.med.upenn.edu.

[2] The abbreviations used are: PHD, prolyl hydroxylase domain protein; HIF, hypoxia inducible factor; VHL, von Hippel Lindau protein; α-SMA, anti-smooth muscle α-actin; PCNA, proliferating cell nuclear antigen; Et-1, endothelin-1; EPO, erythropoietin; DIG, digoxigenin.

sac, Hif-1α is essential for proper signaling through the Epo/EpoR axis (15). In adult mice, studies employing genetically modified mice have identified Hif-2α as being the critical isoform (16–18). These studies lead to the question of whether human mutations in *HIF* genes might be associated with erythrocytosis. We recently identified a heterozygous gain of function missense mutation in the *HIF2A* gene associated with erythrocytosis (19). This mutation, G537W, is in the vicinity of the primary site of hydroxylation. *In vitro*, the mutation impairs the ability of HIF-2α to be hydroxylated by PHD2 and to then be recognized by VHL. Multiple, additional mutations in the *HIF2A* gene associated with erythrocytosis have subsequently been identified (20–23). These mutations are all heterozygous missense mutations that change amino acids that are in close proximity to the primary site of hydroxylation, Pro-531. It remains conceivable that these mutations are polymorphisms unrelated to the phenotype. Therefore, in the present report, we generated a *Hif2a* knock-in mouse to model the original *HIF2A* mutation. This model provides an opportunity to not only test whether a single amino acid change in Hif-2α is sufficient to induce erythrocytosis, but also examine whether there are other sequelae from this global dysregulation of Hif-2α function.

EXPERIMENTAL PROCEDURES

Gene Targeting—The construct for generating a G536W mutation in the mouse *Hif2a* gene was prepared by recombineering (24). In brief, a minitargeting vector was constructed in the vector pL452 (25). This minitargeting vector contained genomic DNA encompassing exon 12 of the mouse *Hif2a* gene with nucleotide changes encoding for the G536W mutation. A silent, diagnostic XhoI site was introduced upstream of the mutation. The vector contained a neomycin selection cassette flanked by loxP sites, and additional sequences downstream of exon 12. A retrieval plasmid was constructed in the vector pMC1-DTA (26). This retrieval plasmid contained sequences that flank 12 kb of genomic DNA sequence at the mouse *Hif2a* locus, as well as a diptheria toxin A negative selection cassette. This retrieval plasmid was used to capture, by recombineering, 12 kb of mouse *Hif2a* genomic DNA containing exons 8 to 16 from C57BL/6 bacterial artificial chromosome clone RP23–106L19 (Invitrogen). The resulting product was used, in the second recombineering step with the minitargeting vector, to generate the final targeting vector. This targeting vector contains an 8.6-kb 5′ arm containing exon 12 with the G536W knock-in mutation, a neomycin selection cassette flanked by loxP sites, and a 3.3-kb 3′ arm (Fig. 1). The presence of the knock-in mutation as well as the integrity of all exons was confirmed by DNA sequencing.

C57BL/6 ES cells were electroporated with the targeting vector and selected using G418 by Caliper Life Sciences. Screening was performed by Southern blotting. Of 192 clones, 9 potential targeted clones were identified. Sequencing of five of these clones revealed that all five had the G536W heterozygous mutation. Two of these clones were injected into C57BL/6 blastocysts to produce chimeras. Chimeric male mice were then mated with C57BL/6 female mice, and germline transmission (assessed by PCR and Southern blotting) was obtained with chimeras derived from both of the targeted ES clones. Mice with germline transmission of the knock-in allele were then mated with C57BL/6-Gt(*ROSA)26Sor*$^{tm16(Cre)Arte}$ mice (Taconic) to delete the neomycin cassette, followed by further crossing with C57BL/6 mice to segregate the *Cre* allele, thereby creating *Hif2a*$^{G536W/+}$ mice. These mice were maintained in a C57BL/6 background. All animal procedures were approved by the Institutional Animal Care and Use Committees at the University of Pennsylvania in compliance with Animal Welfare Assurance.

Southern Blotting—Digoxigenin-labeled probes were generated by PCR using a PCR DIG Probe Synthesis Kit (Roche Applied Science). For the 5′ probe (0.7 kb), the primers were 5′-GTG TGC ATG CGG GAG AGC CT-3′ and 5′-TGA GCT CGA GCT CTC CCG ACT GTA-3′. For the 3′ probe (0.45 kb), the primers were 5′-CTA AAA GCT TAG AAA TGG GAT CTT GC-3′ and 5′-TTA TGA ATT CCC ATT AAA AAC ATT TC-3′. For both probes, DNA derived from bacterial artificial chromosome clone RP23–106L19 was employed as the template. Southern blotting was performed using DIG Easy Hyb, DIG wash and block buffer set, anti-digoxigenin-AP conjugates, and CDP-Star substrate (Roche Applied Science).

PCR Genotying—DNA was isolated from mouse tails (27). The following primers were employed for genotyping the G536W knock-in mutation: Hex12-2 5′ = 5′-GTC TTC CAT CTT CTT TGA TGC TGG-3′ and Hint12-3 3′ = 5′-ACA CAT CAG CTT ATG GGA CTG CAG-3′. The wild type allele produces a PCR product of 0.60 kb, whereas the knock-in mutant allele produces a PCR product of 0.66 kb.

Hematologic, Epo, and Vegf Measurements—Hematocrit, hemoglobin, and complete blood counts were measured on retroorbital blood samples as previously described (28). Serum was obtained by centrifugation at 2,000 × *g* for 20 min. Serum Epo and Vegf-a levels were measured using ELISA kits (R & D Systems).

Real-time PCR Analysis—Total RNA was isolated from kidney, liver, lung, bone, and brain tissues by using TRIzol reagent. One μg of total RNA was used for reverse transcription. Twenty ng eq of cDNA was used for SYBR Green Real-time PCR analysis. The sequences of the primers employed for Real-time PCR analysis are provided in the Table 1. Relative quantification was performed employing the $\Delta\Delta C_t$ method and 18S RNA as the endogenous control.

Histologic Analysis—Lungs were inflated by injection of 10% buffered formalin through the trachea and placed in 10% buffered formalin for fixation, and then embedded in paraffin. Immunohistochemistry was performed by standard protocols. After deparaffinization/rehydration and antigen retrieval, the slides were stained with rabbit anti-smooth muscle α-actin (α-SMA) (1:500, Genetex catalog number 100034) or anti-proliferating cell nuclear antigen (PCNA) (1:200, Genetex catalog number 100539), biotinylated goat anti-rabbit antibody (1:200, BD Pharmingen), and streptavidin-horseradish peroxidase (BD Pharmingen).

Vascular changes in pulmonary arteries identified in α-SMA-stained lung tissues were assessed by percent medial thickness as previously described (29). The medial thickness and the external diameter were measured using NIH ImageJ

TABLE 1
Primer sequences employed for RT-PCR

Gene	Forward primer	Reverse primer
Epo	CATCTGCGACAGTCGAGTTCTG	CACAACCCATCGTGACATTTTC
Vegfa	TACCTCCACCATGCCAAGTG	TGGGACTTCTGCTCTCCTTCTG
18S	TCGGAACTGAGGCCATGATT	TAGCGGCGCAATACGAATG
Pgk-1	GGAAGCGGGTCGTGATGA	GCCTTGATCCTTTGGTTGTTTG
Et-1	GCTGGTGGAAGGAAGGAAACTAC	AAAAGATGCCTTGATGCTATTGC
Pdgfb	CGCACAGAGGTGTTCCAGATC	CCAGGAAGTTGGCGTTGGT
Sdf-1	CCCTGCCGGTTCTTCGA	GAGGATTTTCAGATGCTTGACGTT
Serpine	CGACACCCTCAGCATGTTCA	CGGAGAGGTGCACATCTTTCT
Arginase II	GATTGATCGACTTGGGATCCA	TGCCAATCAGCCGATCAAA
Retnla	TCGTGGAGAATAAGGTCAAGGAA	TCTTCGTTACAGTGGAGGGATAGTT
Fhl-1	GGCACCGTCTGGCATAAAGA	CCGGTCCCAATGACTTGCT

software (imagej.nih.gov/ij/). The % medial thickness was calculated for at least 40 small pulmonary arteries (from 20 to 80 μM) for each mouse. Circular or near circular vessels were chosen for analysis.

Vessel muscularity was determined using α-SMA-stained lung sections, with at least 60 small pulmonary arteries scored per animal. The number of fully muscular (completely circumferential α-SMA staining), partially muscular (partially circumferential α-SMA staining), or non-muscular (no α-SMA staining) vessels were counted and the percentage of each category calculated. For PCNA immunostaining, 12–20 small pulmonary arteries were analyzed per mouse.

Pulmonary Function Tests—Pulmonary function was assessed by plethysmography. The mice were placed into a 150-ml whole body plethysmograph connected to a pneumotachometer and the difference of pressure integrated in a Spirometer (ADInstruments). The O_2 concentration in the chamber was controlled by a Pegas-400 MF Gas Mixer (Columbus Instruments). Respiration data for mice under normoxia (21% O_2) or hypoxia (12% O_2) were recorded using a PowerLab 8/SP instrument (ADInstruments) and analyzed with LabChart 6 software (ADInstruments). Ventilatory frequency (*f*), tidal volume V_T (μl), and minute ventilation V_E (μl/min) were measured. Calibration was performed according to the manufacturer's manual.

Echocardiography and Right Ventricular Pressure Measurements—For right ventricular pressure measurements, mice were anesthetized by isoflurane inhalation, placed in the supine position, and a midline cervical incision was made to expose the right jugular vein by microsurgical techniques. A 1.4 French miniaturized pressure catheter (Millar instruments) was inserted via the right jugular vein and advanced to the right ventricle chamber for the measurement of right ventricle pressure and heart rate. Data were recorded and analyzed using PowerLab equipment (ADInstruments) and LabChart 6 software.

For echocardiography, an ultra-high frequency small animal ultrasound system was used. This consisted of a Vevo 770 ultrasound system (VisualSonics Inc., Toronto, ON, Canada) equipped with a 30-MHz probe (RMV-707B), with an attached Integrated Rail System III for image acquisition. Mice were anesthetized with isoflurane. All measurements were analyzed by using the Vevo 770 Standard Measurement Package.

Arterial Blood Gas Measurements—Blood from the carotid artery was drawn into a heparin-lined syringe and analyzed using an i-STAT instrument equipped with G3+ cartridges (Abbott Laboratories). Blood oxygen saturation (SaO_2) measurements were obtained on awake (unanesthetized) animals using a non-invasive pulse oximeter collar (Starr Life Sciences) placed over the carotid arteries of the mice. Mice were allowed to walk freely in a small chamber while measurements were taken. A minimum of 3 min of continuous recording was obtained.

Core Body Temperature Measurements—Rectal temperature was measured at room temperature using a thermistor (YSI Model 4600).

Statistical Analysis—Data were analyzed by analysis of variance or by unpaired Student's *t* test. *p* values below 0.05 were considered significant. Data are presented as mean ± S.E.

RESULTS

We generated a *Hif2a* G536W knock-in mutation in a C57BL/6 background. The targeting strategy is shown in Fig. 1*A*. The targeting vector contains 5′ and 3′ homology arms, as well as neomycin positive selection and diphtheria toxin A negative selection cassettes. Following electroporation into C57BL/6 ES cells and selection using G418, clones with the correct recombination event and mutation were identified. Southern blotting with a 5′ probe revealed the expected 9.5-kb band upon hybridization with SphI-digested DNA in addition to the wild type 12-kb band (Fig. 1*B*, *left panel*, *lane 2*). Southern blotting with a 3′ probe revealed the expected 7.8-kb band upon hybridization with XhoI-digested DNA in addition to the wild type 11.1-kb band (Fig. 1*B*, *right panel*, *lane 2*). Sequencing confirmed the presence of a heterozygous G536W mutation in the *Hif2a* gene (Fig. 1*C*). Chimeras were derived and germline transmission was obtained, as assessed by Southern blotting (Fig. 1*B*, *left* and *right panels*, *lane 3*). The neomycin cassette was deleted and confirmed by Southern blotting (Fig. 1*B*, *left panel*, compare *lanes 3* and *5*). A PCR genotyping strategy was developed (Fig. 1*D*).

We mated $Hif2a^{G536W/+}$ mice and were able to obtain both $Hif2a^{G536W/+}$ and $Hif2a^{G536W/G536W}$ mice, with the latter at a frequency (13%) lower than the expected (25%) Mendelian frequency (Table 2), suggesting that homozygosity of the mutation confers a survival disadvantage during embryogenesis. Notably, the homozygous mouse survival at 18 months (6/6 mice) was the same as that of either heterozygote (10/10) or wild type mice (10/10). We also measured body weights and did not observe any significant differences between the three groups over a 5-month period of observation (data not shown).

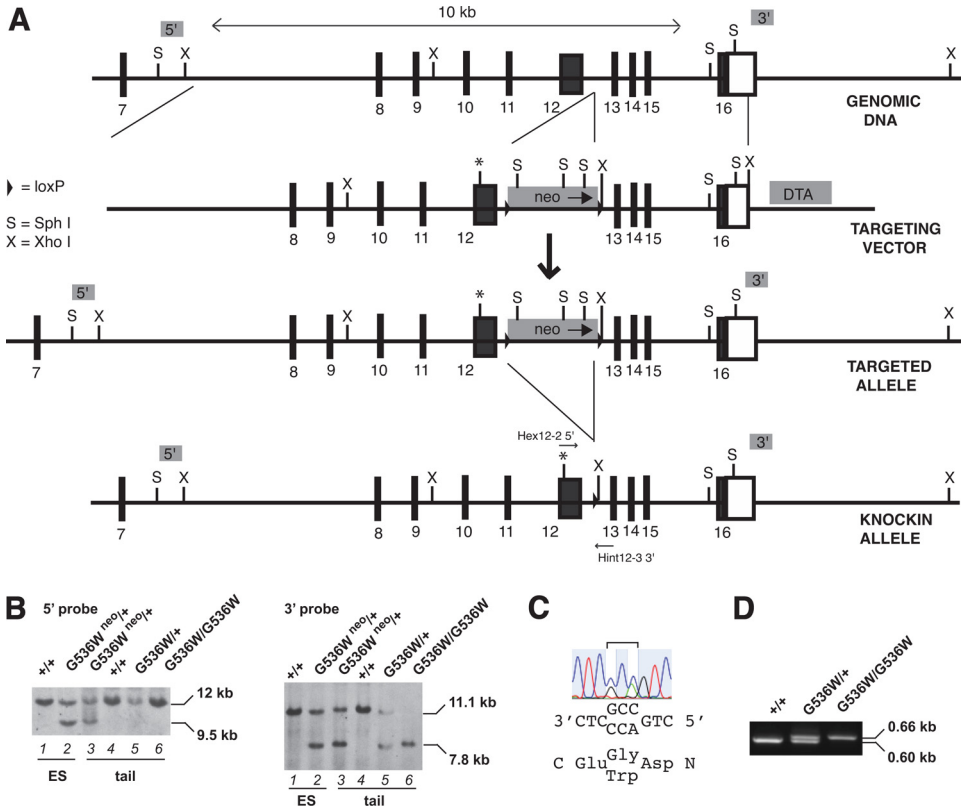

FIGURE 1. **Generation of *Hifa* G536W knock-in mice.** *A,* gene targeting strategy for introduction of *Hif2a* G536W mutation. The *asterisk* indicates the G536W mutation. *Black boxes* indicate exons, with the exon number indicated beneath the box. *Open box* indicates the 3′ untranslated region. *DTA* and *neo* denote diphtheria toxin A and neomycin cassettes, respectively. Positions of Hex12-2 5′ and Hint 12-3 3′ PCR primers are shown. *B,* Southern blots employing 5′ (*left*) and 3′ (*right*) probes of SphI- or XhoI-digested DNA, respectively, of ES cell or mouse tail DNA. *Hif2a* genotypes are provided at the *top*. The presence of the neomycin cassette is denoted by *neo*. *C,* DNA sequencing chromatogram of targeted ES cell DNA. The sequence is from 3′ to 5′ (reverse complement). The codon at residue 536 is in the middle and is heterozygous for Gly (GGC) and Trp (TGG). *D,* PCR genotyping of *Hif2a* knock-in mice by using Hex12-2 5′ and Hint 12-3 3′ primers. The 0.60-kb product is derived from the wild type allele, whereas the 0.66-kb product is derived from the G536W mutant allele. *Hif2a* genotypes are shown at the *top*.

TABLE 2

Genotypes of pups from *Hif2a*$^{G536W/+}$ intercrosses

In parentheses, the number observed with the indicated genotype/total number is shown.

Genotype	Expected	Observed
	%	
Hif2a$^{G536W/G536W}$	25	13 (31/240)
Hif2a$^{G536W/+}$	50	50 (120/240)
Hif2a$^{+/+}$	25	37 (89/240)

We measured hematocrit and hemoglobin levels in these mice and observed increased levels of both parameters in both the *Hif2a*$^{G536W/+}$ and *Hif2a*$^{G536W/G536W}$ mice as compared with wild type mice (Fig. 2, *A* and *B*). For hematocrit, the values (mean ± S.E.) were 48.9 ± 0.38, 53.6 ± 0.64, and 57.1 ± 1.7% for *Hif2a*$^{+/+}$, *Hif2a*$^{G536W/+}$, and *Hif2a*$^{G536W/G536W}$ mice, respectively. For hemoglobin, the values were 15.2 ± 0.16, 16.8 ± 0.17, and 17.7 ± 0.41 g/dl for *Hif2a*$^{+/+}$, *Hif2a*$^{G536W/+}$, and *Hif2a*$^{G536W/G536W}$ mice, respectively. The red blood cell counts were also increased in a mutation dose-dependent manner (Fig. 2*C*).

We measured platelet and white blood cell counts (Fig. 2, *D* and *E*, respectively). There was no significant difference in platelet counts between the three groups. We did observe changes in white blood cell counts in *Hif2a*$^{G536W/+}$ as compared with wild type mice. The white blood cells were 12.5 ± 0.63, 16.3 ± 1.2, and 15.9 ± 1.4 K/μl for *Hif2a*$^{+/+}$, *Hif2a*$^{G536W/+}$, and *Hif2a*$^{G536W/G536W}$ mice, respectively. When individual components of the white blood cell population were examined, we observed increases in lymphocytes and monocytes in *Hif2a*$^{G536W/+}$ mice, and in monocytes in *Hif2a*$^{G536W/G536W}$ mice (Fig. 2*F*). Others have noted functional effects of Epo on macrophages (30). We measured serum Epo levels and did not observe a statistically significant increase in Epo levels in heterozygous compared with wild type mice (Fig. 3*A*). However, Epo levels were increased in homozygous mice as compared with wild type mice or heterozygous mice. For the *Hif2a*$^{+/+}$ and *Hif2a*$^{G536W/G536W}$ mice, the values were 158 ± 14 and 282 ± 22 pg/ml, respectively.

We measured *Epo* mRNA levels in the kidneys by real-time PCR (Fig. 3*B*). Although there was a trend toward an increase in *Epo* message with increasing mutation dose, the results were not statistically significant. We also examined other tissues that are potential sources of Epo (8–10). Compared with kidney, substantially lower levels of *Epo* mRNA were detected in the brain. In this organ, levels of *Epo* message were increased in the *Hif2a*$^{G536W/+}$ and *Hif2a*$^{G536W/G536W}$ mice (Fig. 3*B*). We did not observe significant differences in levels of *Epo* message in the liver, which in all cases were substantially lower than that seen in the kidney (Fig. 3*B*). Furthermore, we could not detect *Epo* message in the bone (data not shown).

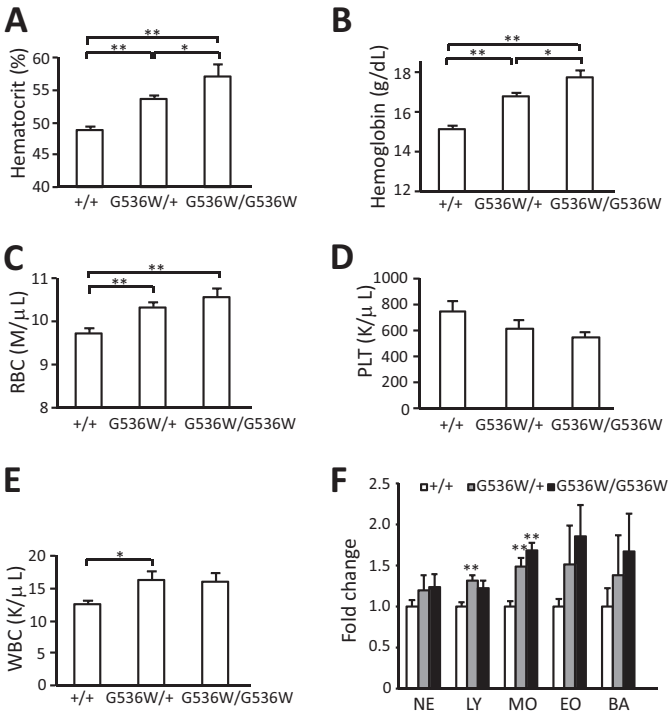

FIGURE 2. ***Hif2a*$^{G536W/+}$ and *Hif2a*$^{G536W/G536W}$ mice display erythrocytosis.** *A,* hematocrit; *B,* hemoglobin; *C,* red blood cell; *D,* platelet; and *E,* white blood cell counts were measured in blood obtained from mice with the indicated *Hif2a* genotypes (age = 1–3 months; $n = 6$–10 per group). *F,* the neutrophil (*NE*), lymphocyte (*LY*), monocyte (*MO*), eosinophil (*EO*), and basophil (*BA*) concentrations were measured and normalized to that of wild type mice. The data are presented as mean ± S.E. * indicates $p < 0.05$, and ** indicates $p < 0.01$.

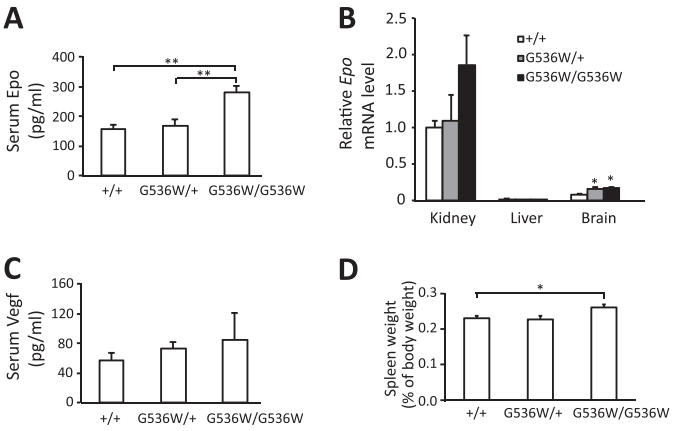

FIGURE 3. ***Hif2a*$^{G536W/G536W}$ mice display increased serum Epo.** *A*, Epo concentrations in serum were measured by ELISA (age = 3–8 months; $n = 4$–10 per group). *B*, *Epo* mRNA levels in the indicated organs at 6–8 months of age were determined by real-time PCR, and normalized to that of 18S rRNA ($n = 4$). The data are presented as the fold-change in reference to mRNA levels in kidneys of wild type mice. In *B*, there was a trend toward an increase of renal *Epo* mRNA in Hif-2$\alpha^{G536W/G536W}$ mice as compared with wild type mice, but it was not statistically significant ($p = 0.13$). The data are presented as mean ± S.E. * indicates $p < 0.05$, and ** indicates $p < 0.01$. *C*, Vegf concentrations in serum were measured by ELISA (age = 3–8 months; $n = 4$–10 per group). *D,* spleen weights were measured in mice with indicated *Hif2a* genotypes (age = 16–19 months; $n = 3$–6 per group). * indicates $p < 0.05$.

Serum Vegf levels were also measured (Fig. 3*C*). No significant differences were seen among the three genotypes. We measured *Vegfa* mRNA levels and did not observe any significant differences in kidney, liver, or lung (data not shown). Spleen weights of *Hif2a*$^{G536W/G536W}$ mice were slightly increased (Fig. 3*D*). We did not observe changes in the weights of livers, kidneys, or lungs (data not shown).

Mice with constitutive activation of the Hif pathway due to liver-specific knock-out of *Vhl* display steatosis and hemangiomas that are Hif-2α dependent (31, 32), whereas other mice with renal proximal tubule-specific knock-out of *Vhl* display renal cysts that are Hif-2α dependent (33). We therefore conducted histologic examinations of the livers and kidneys of these mice. Although there were focal areas of microsteatosis in some of the heterozygous or homozygous mice, these areas were not increased in incidence compared with wild type mice (data not shown). Similarly, examination of the kidneys failed to reveal the presence of cysts in either *Hif2a*$^{G536W/+}$ or *Hif2a*$^{G536W/G536W}$ mice (data not shown).

Abnormalities in pulmonary function have been observed in HIF dysregulation due to the Chuvash mutation in the *VHL* gene (34, 35). We therefore measured the respiratory frequency (f), tidal volume (V_T), and minute ventilation (V_E) of these mice under normoxic and hypoxic (12% O_2) conditions (Fig. 4). Under normoxic conditions, no differences were seen in any of the parameters. Under hypoxic conditions, we find that *Hif2a*$^{G536W/G536W}$ mice display an increase in respiratory frequency when compared with either heterozygote or wild type mice (Fig. 4*A*). Of note, studies of human patients with gain of function *HIF2A* mutations reveal no changes in minute ventilation under either normoxic or hypoxic conditions; however, they do display increased ventilation relative to metabolism (as reflected by the ratio of arterial to end tidal P_{CO2}) (36).

Dysregulation of the HIF pathway has also been reported to result in pulmonary hypertension both in mouse models and in some human patients with *HIF2A* mutations (21, 34, 35). We therefore measured right ventricular heart pressure by cardiac catheterization, and right ventricular wall thickness by echocardiography (Fig. 5). We find a significant increase in right ventricular pressure in heterozygotes, with an even more dramatic increase in homozygotes. The right ventricular pressures were 28.3 ± 2.3, 45.9 ± 1.1, and 65.7 ± 10.1 mm Hg for *Hif2a*$^{+/+}$, *Hif2a*$^{G536W/+}$, and *Hif2a*$^{G536W/G536W}$ mice, respectively (Fig. 5*A*). These measurements were made in mice that were 16 to 19 months of age. We also examined *Hif2a*$^{G536W/G536W}$ mice at 4 to 6 months of age, and observed pulmonary hypertension at this age as well (25.6 ± 1.2 and 41.8 ± 1.4 mm Hg for *Hif2a*$^{+/+}$ and *Hif2a*$^{G536W/G536W}$ mice, respectively; Fig. 5*B*). The degree of pulmonary hypertension in the younger mice was less than that seen in the older ones, suggesting an age-dependent effect on this phenotype.

Measurements of right ventricular wall thickness by echocardiography show increases in *Hif2a*$^{G536W/G536W}$ mice under either systole or diastole (Fig. 5, *C* and *D*). For example, under systole, the right ventricular thickness was 0.40 ± 0.02 and 0.61 ± 0.03 mm for *Hif2a*$^{+/+}$ and *Hif2a*$^{G536W/G536W}$ mice, respectively. No changes were seen in right ventricular inner diameter, main pulmonary artery inner diameter, or in heart rate (Fig. 5, *E* and *F*, and data not shown). The heart/body weight ratio was increased in *Hif2a*$^{G536W/G536W}$ mice. It was 0.498 ± 0.020 and 0.654 ± 0.023% for *Hif2a*$^{+/+}$ and *Hif2a*$^{G536W/G536W}$ mice, respectively (Fig. 5*G*).

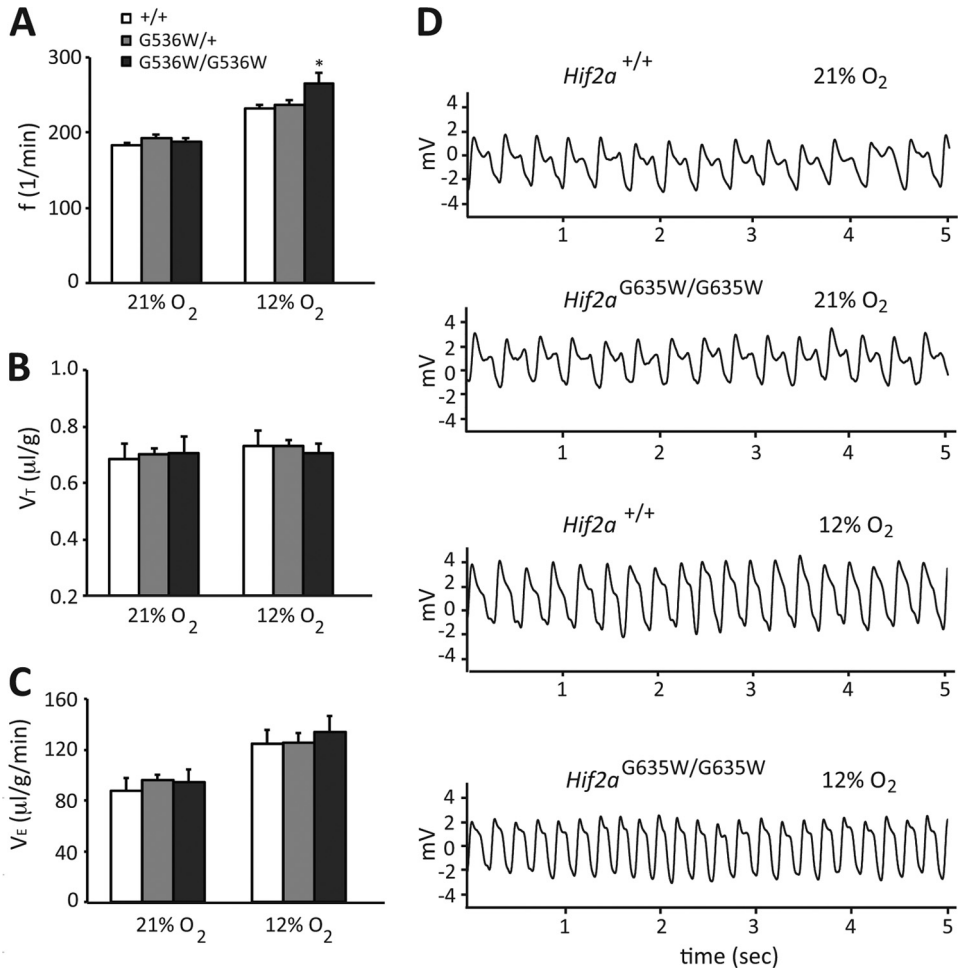

FIGURE 4. **Pulmonary function parameters in *Hif2a*$^{G536W/+}$ and *Hif2a*$^{G536W/G536W}$ mice.** The respiratory frequency, *f* (*A*), tidal volume V_T (*B*), and minute ventilation V_E (*C*) of wild type, *Hif2a*$^{G536W/+}$, and *Hif2a*$^{G536W/G536W}$ mice (age = 10–17 months; $n = 3–5$ per group) under normoxic (21% O_2) and hypoxic (12% O_2) conditions were measured. V_T and V_E were normalized to body weight. * indicates $p < 0.05$ in comparison to either wild type or *Hif2a*$^{G536W/+}$ mice. *D*, representative plethysmography traces for wild type and *Hif2a*$^{G536W/G536W}$ mice under normoxic and hypoxic conditions.

Patients with gain of function mutations in the *HIF2A* gene display decreased $PaCO_2$ but not PaO_2 or pH compared with controls (36). We measured arterial blood gases in *Hif2a*$^{+/+}$ and *Hif2a*$^{G536W/G536W}$ mice, and did not observe any significant differences in these or other parameters (Table 3). There was no difference in oxygen saturation between these two genotypes. We also measured core body temperature, and did not observe any difference between *Hif2a*$^{+/+}$ and *Hif2a*$^{G536W/G536W}$ mice (37.72 ± 0.31 and 38.25 ± 0.11 °C, respectively, $n = 4$).

Histologic examinations of the lungs revealed a slight increase in the thickness of small pulmonary arteries in *Hif2a*$^{G536W/G536W}$ mice as compared with wild type mice (Fig. 6, *A* and *B*). We also determined the proportions of fully, partially, and non-muscularized small pulmonary arteries, and observed a decrease in the non-muscularized arteries in *Hif2a*$^{G536W/G536W}$ mice as compared with wild type mice (Fig. 6*C*).

Pulmonary hypertension, in general terms, can be due to a number of different pathophysiologic processes, including imbalances between pulmonary arterial vasoconstrictors and vasodilators, and inappropriate proliferation of smooth muscle cells (37–39). Immunostaining for PCNA revealed occasional PCNA-positive smooth muscle cells in small pulmonary arteries of *Hif2a*$^{G536W/G536W}$ mice (Fig. 6*D*). However, these were not present in significantly different numbers compared with *Hif2a*$^{+/+}$ controls (Fig. 6*E*), suggesting that changes in the mitotic rate of smooth muscle cells alone cannot account for the increased thickness.

Mediators of pulmonary hypertension that have been identified include the vasoconstrictor endothelin-1 (Et-1) and the smooth muscle mitogen Pdgf-β. Other genes have been implicated as well, including those encoding for the chemokine Sdf-1 (also known as Cxcl12), the prothrombotic protein Serpine (also known as Pai), Arginase II, Retnla (also known as fizz1), and Fhl-1 (40–44). A number of these genes are Hif-target genes (35). We examined these genes by real-time PCR (Fig. 6*F*). We observe substantial increases in *Et-1*, *Pdgfb*, and *Sdf-1* mRNA in lungs from *Hif2a*$^{G536W/G536W}$ mice compared with wild type. No significant differences were observed in the levels of expression of the other target genes, nor in the canonical Hif-1α target gene *Pgk-1* (Fig. 6*F*), which was not elevated in either liver or kidney (data not shown).

DISCUSSION

The HIF pathway is the central pathway governing the transcriptional response to hypoxia (6). The present mouse model

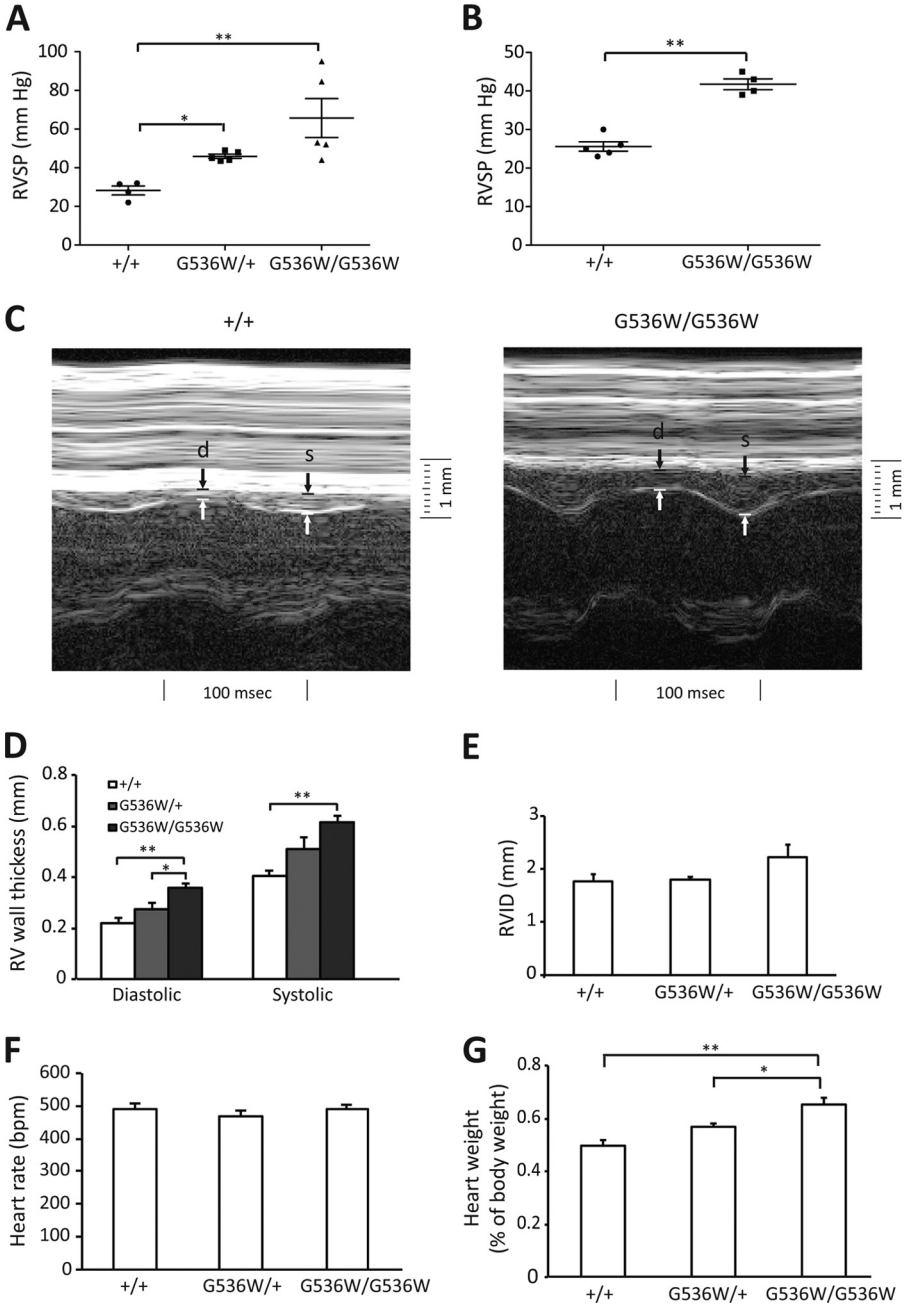

FIGURE 5. ***Hif2a*$^{G536W/+}$ and *Hif2a*$^{G536W/G536W}$ mice develop pulmonary hypertension and right ventricular hypertrophy.** *A* and *B*, right ventricular systolic pressure; *D*, right ventricular wall thickness in diastole or systole; *E*, right ventricular inner diameter (*RVID*); *F*, heart rate; and *G*, heart weight (as a percentage of total body weight) were measured in mice with the indicated *Hif2a* genotypes (age = 16–19 months, $n = 4–7$ per group for *panels A* and *D–G*; age = 4–6 months, $n = 4–5$ per group for *panel B*). *C*, representative M-mode echocardiographs for mice with the indicated *Hif2a* genotypes. Right ventricular wall thickness in diastole and systole are indicated by *d* and *s*, respectively. In *A*, due to the variability in data for the homozygous mice, data were subjected to log transformation prior to analysis of variance. * indicates $p < 0.05$, and ** indicates $p < 0.01$.

TABLE 3

Arterial blood gas analysis of *Hif2a*$^{+/+}$ and *Hif2a*$^{G536W/G536W}$ mice

Shown are mean ± S.E. $n = 4$ - 6 per group (4 to 6 months of age). No significant differences were seen between the two groups ($p > 0.05$ for all parameters).

	Hif2a$^{+/+}$	*Hif2a*$^{G536W/G536W}$
pH	7.28 ± 0.023	7.29 ± 0.061
$PaCO_2$	36.7 ± 2.0	29.8 ± 3.7
PaO_2	85.3 ± 3.4	91.8 ± 2.2
HCO_3^-	18.2 ± 0.6	14.9 ± 2.1
TCO_2	19.3 ± 0.7	16.0 ± 2.3
BE_{ecf}	−9.0 ± 1.0	−12.5 ± 2.5
SaO_2	96.5 ± 0.59	96.4 ± 0.81

provides an opportunity to examine the consequences of global expression of a hypermorphic *Hif2a* allele both in a heterozygous state that models a human disease, as well as in a homozygous state that is not known to occur in humans. Notable features of this mouse model are: 1) it introduces a gain of function allele, as opposed to a hypomorphic or knock-out allele, 2) it is globally expressed from its endogenous locus, and 3) it is selective for one, as opposed to both, Hif-α isoforms. The two most striking findings are the marked erythrocytosis and dramatic pulmonary hypertension, both of which were observed with

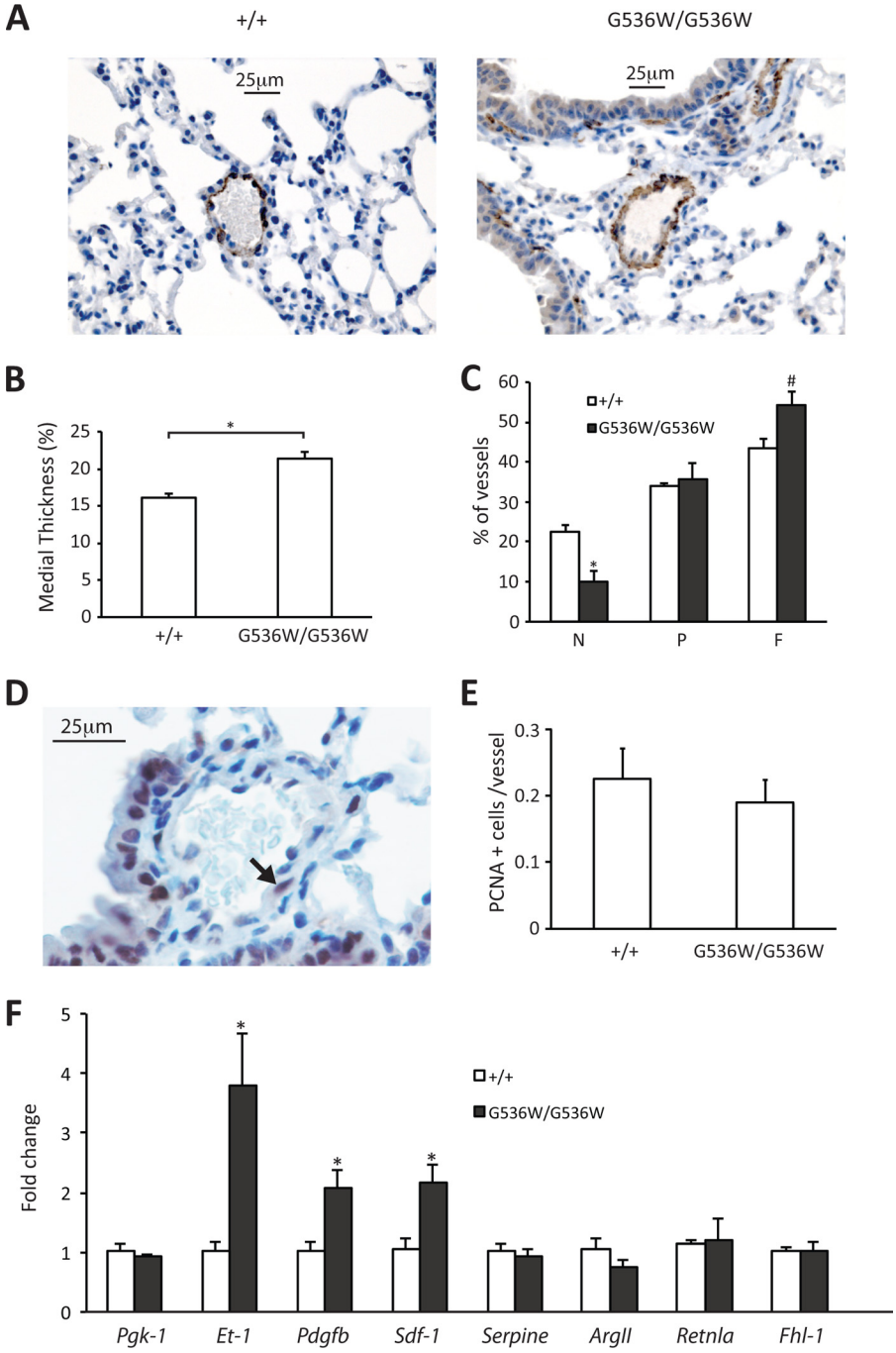

FIGURE 6. **Up-regulation of *Et-1* and *Pdgfb* mRNA in *Hif2a*$^{G536W/G536W}$ mice.** *A*, photomicrographs of immunoperoxidase-stained sections of lungs from wild type and *Hif2a*$^{G536W/G536W}$ mice (magnification = ×400) using antibodies against smooth muscle actin. Small pulmonary arteries are in the center of each photomicrograph. *Bars* indicate 25 μM. *B*, the medial thickness of small pulmonary arteries (expressed as a percentage of the external diameter), and *C*, the proportions of non-muscularized (*N*), partially muscularized (*P*), and fully muscularized (*F*) pulmonary arteries were measured in lungs obtained from mice with the indicated genotypes (age = 10–17 months; $n = 3$ per group). *D*, photomicrograph of the immunoperoxidase-stained section of lung from *Hif2a*$^{G536W/G536W}$ mice using antibodies against PCNA. A PCNA-positive smooth muscle cell is indicated by the *arrow*. *E*, numbers of PCNA-positive smooth muscle cells in small pulmonary arteries of wild type and *Hif2a*$^{G536W/G536W}$ mice (age = 10–17 months; $n = 3$ per group). *F*, the levels of the indicated mRNAs in lung were determined by real-time PCR ($n = 4$). Mice were 6–8 months. The data are presented as the fold-change in reference to mRNA levels in wild type mice. * indicates $p < 0.05$ in comparison to wild type mice. In *C*, # indicates $p = 0.08$ in comparison to wild type mice.

high penetrance, and both of which occur in a mutation dose-dependent manner.

The pulmonary hypertension in *Hif2a* knock-in mice could, in principle, be due to the erythrocytosis. However, the following observations argue against this. In other studies, mice with a heterozygous loss of function mutation in *Phd2* (P294R), which models a human erythocytosis-associated PHD2 mutation (P317R), exhibited increased hematocrit and hemoglobin levels[3] that are comparable with that seen in the *Hif2a*$^{G536W/+}$

[3] P. Arsenault, personal communication.

mice. However, in contrast to *Hif2a*$^{G536W/+}$ mice, these *Phd2* knock-in mice did not develop pulmonary hypertension. In addition, mice with transgenic overexpression of EPO develop erythrocytosis (Hct >80%) that is even more severe than that observed with the *Hif2a*$^{G536W/G536W}$ mice, yet they do not develop pulmonary hypertension (45).

Pulmonary hypertension has been observed in patients with Chuvash polycythemia, in a mouse model of Chuvash polycythemia, and in some patients with *HIF2A* erythrocytosis-associated mutations (21, 34, 35, 46). Heterozygosity of *Hif2a* deletion reverses the pulmonary hypertension seen in mice bearing the Chuvash mutation as well as that induced by chronic hypoxia, indicating that pulmonary hypertension is at least, in part, *Hif2a*-dependent (35, 47). Those mouse studies provided compelling evidence that *Hif2a* is necessary, but left open the question of whether it alone is sufficient for the development of pulmonary hypertension. The present findings show that in a mouse model, a single missense mutation in Hif-2α is indeed sufficient to induce pulmonary hypertension. This observation is all the more notable given the fact that mutation is a partial, as opposed to complete, gain of function. For example, *in vitro* studies indicate that the G537W mutation stabilizes HIF-2α, but does so less effectively than mutation of the primary hydroxylacceptor proline, Pro-531 (48). Real-time PCR analysis identifies genes, *Et-1*, *Pdgfb*, and *Sdf-1*, that are up-regulated in these mice. It is plausible that Hif-2α up-regulates a panel of genes, including those just mentioned, that in turn mediate the development of pulmonary hypertension.

Epo protein levels were elevated in the serum obtained from the *Hif2a*$^{G536W/G536W}$ homozygotes, but not *Hif2a*$^{G536W/+}$ mice. Most patients with erythrocytosis-associated *HIF2A* mutations display elevated EPO levels, although it might be noted that some display normal EPO levels (23, 49). It is conceivable that Hif-2α may have effects on either the bone marrow microenvironment (50) or on erythroid precursors (11), possibilities that will require further investigation. Interestingly, the *Hif2a*$^{G536W/G536W}$ homozygous mice do not display a statistically significant increase in their Epo mRNA levels in their kidneys. It is reasonable to speculate that elevated serum Epo in *Hif2a*$^{G536W/G536W}$ mice may be from the contribution of several organs in these mice with this global hypermorphic *Hif2a* mutation. For example, there may be a contribution to circulating Epo from the brain, which does display increased *Epo* mRNA levels in *Hif2a*$^{G536W/G536W}$ mice (Fig. 3*B*). The liver might be considered another potential source; however, we were not able to detect any significant changes in the *Epo* mRNA level in this tissue, which was low in comparison to the levels seen in the kidney.

It is noteworthy that the knock-in mice did not display certain stigmata of dysregulation of the HIF pathway seen in other contexts. For example, conditional knock-out of *Vhl* in the mouse liver results in hemangiomas and steatosis that are reversed by concurrent deletion of *Hif2a*, whereas conditional knock-out of *Vhl* in the kidney results in cysts that are absent when *Hif2a* is concurrently deleted (31–33). Patients with Chuvash polycythemia display an increased incidence of vertebral hemangiomas (51). Moreover, conditional expression of a strongly constitutively active HIF-2α (P405A/P531A) in the mouse liver results in hemangiomas (52). Possible explanations for our present results in comparison to previous ones are as follows: 1) Hif-2α expression may be necessary but not sufficient for the development of these lesions, 2) there may be Hif-independent functions of Vhl, and 3) the G536W gain of function mutation in Hif-2α, even in its homozygous state, may not be as strong as that induced by *Vhl* ablation or the P405A/P531A mutation noted above. As previously mentioned, *in vitro* studies indicate that the G537W mutation in HIF-2α stabilizes HIF-2α to a lesser extent than a P531A mutation (48).

Heterozygous *HIF2A* mutations exist in humans (1), and it is formally possible that these individuals may have modifier genes or compensatory mutations at other gene loci that allow these mutations, which might otherwise be incompatible with viability, to exist in nature. The present studies, which were conducted in a uniform strain background (C57BL/6) argue against this possibility. Specifically, they indicate that constitutive global activation of Hif-2α due to a heterozygous gain of function mutation is compatible with viability in mice. Indeed, mice that are homozygous for the *Hif2a* knock-in mutation are viable as well.

These studies, taken together, indicate that a missense mutation in one Hif-α isoform is sufficient to produce significant hematopoietic and cardiopulmonary phenotypes, although interestingly, it does not recapitulate all of the sequelae that have been observed due to HIF-α dysregulation in other contexts. There is currently great interest in manipulating the HIF pathway for therapeutic benefit in ischemic diseases and anemia (4). The current studies provide valuable information for strategies that seek to selectively up-regulate the HIF-2α isoform. Conversely, these studies also highlight HIF-2α as a potential therapeutic target for the treatment of pulmonary hypertension (35, 47).

Acknowledgments—We thank Paul Furlow for excellent assistance in generating the Hif2a$^{G536W/+}$ *mouse line, Dr. Liu Xi of the Penn Cardiovascular Institute Mouse Cardiovascular Physiology and Microsurgery Core for performing the echocardiography measurements, Dr. Ravindra Dhir of the Penn Diabetes Research Center Mouse Phenotyping, Physiology, and Metabolism Core for performing the rectal temperature measurements, Evguenia Arguiri for assistance with the arterial blood gas studies, Dr. Emidio Pistilli and Dr. Predrag Krajacic for guidance with the plethysmography, Amy Ziober for providing the unstained slides for immunohistochemistry, and the National Cancer Institute for providing the plasmid pL452 and Escherichia coli SW102 for recombineering. We thank Dr. Patrick Arsenault for comments on the manuscript, Dr. Celeste Simon and Dr. Brian Keith for helpful discussions, and Dr. David B. Roth and Dr. Mark L. Tykocinski for their support.*

REFERENCES

1. Lee, F. S., and Percy, M. J. (2011) The HIF pathway and erythrocytosis. *Annu. Rev. Pathol.* **6,** 165–192
2. Yoon, D., Ponka, P., and Prchal, J. T. (2011) Hypoxia. 5. Hypoxia and hematopoiesis. *Am. J. Physiol. Cell Physiol.* **300,** C1215–1222
3. Wenger, R. H., and Hoogewijs, D. (2010) Regulated oxygen sensing by protein hydroxylation in renal erythropoietin-producing cells. *Am. J. Physiol. Renal Physiol.* **298,** F1287–1296
4. Kaelin, W. G., Jr., and Ratcliffe, P. J. (2008) Oxygen sensing by metazoans.

The central role of the HIF hydroxylase pathway. *Mol. Cell* **30,** 393–402
5. Majmundar, A. J., Wong, W. J., and Simon, M. C. (2010) Hypoxia-inducible factors and the response to hypoxic stress. *Mol. Cell* **40,** 294–309
6. Semenza, G. L. (2007) Life with oxygen. *Science* **318,** 62–64
7. Jelkmann, W. (2007) Erythropoietin after a century of research. Younger than ever. *Eur. J. Haematol.* **78,** 183–205
8. Weidemann, A., Kerdiles, Y. M., Knaup, K. X., Rafie, C. A., Boutin, A. T., Stockmann, C., Takeda, N., Scadeng, M., Shih, A. Y., Haase, V. H., Simon, M. C., Kleinfeld, D., and Johnson, R. S. (2009) The glial cell response is an essential component of hypoxia-induced erythropoiesis in mice. *J. Clin. Invest.* **119,** 3373–3383
9. Rankin, E. B., Wu, C., Khatri, R., Wilson, T. L., Andersen, R., Araldi, E., Rankin, A. L., Yuan, J., Kuo, C. J., Schipani, E., and Giaccia, A. J. (2012) The HIF signaling pathway in osteoblasts directly modulates erythropoiesis through the production of EPO. *Cell* **149,** 63–74
10. Rankin, E. B., Biju, M. P., Liu, Q., Unger, T. L., Rha, J., Johnson, R. S., Simon, M. C., Keith, B., and Haase, V. H. (2007) Hypoxia-inducible factor-2 (HIF-2) regulates hepatic erythropoietin *in vivo*. *J. Clin. Invest.* **117,** 1068–1077
11. Ang, S. O., Chen, H., Hirota, K., Gordeuk, V. R., Jelinek, J., Guan, Y., Liu, E., Sergueeva, A. I., Miasnikova, G. Y., Mole, D., Maxwell, P. H., Stockton, D. W., Semenza, G. L., and Prchal, J. T. (2002) Disruption of oxygen homeostasis underlies congenital Chuvash polycythemia. *Nat. Genet.* **32,** 614–621
12. Percy, M. J., Zhao, Q., Flores, A., Harrison, C., Lappin, T. R., Maxwell, P. H., McMullin, M. F., and Lee, F. S. (2006) A family with erythrocytosis establishes a role for prolyl hydroxylase domain protein 2 in oxygen homeostasis. *Proc. Natl. Acad. Sci. U.S.A.* **103,** 654–659
13. Takeda, K., Aguila, H. L., Parikh, N. S., Li, X., Lamothe, K., Duan, L. J., Takeda, H., Lee, F. S., and Fong, G. H. (2008) Regulation of adult erythropoiesis by prolyl hydroxylase domain proteins. *Blood* **111,** 3229–3235
14. Minamishima, Y. A., Moslehi, J., Bardeesy, N., Cullen, D., Bronson, R. T., and Kaelin, W. G., Jr. (2008) Somatic inactivation of the PHD2 prolyl hydroxylase causes polycythemia and congestive heart failure. *Blood* **111,** 3236–3244
15. Yoon, D., Pastore, Y. D., Divoky, V., Liu, E., Mlodnicka, A. E., Rainey, K., Ponka, P., Semenza, G. L., Schumacher, A., and Prchal, J. T. (2006) Hypoxia-inducible factor-1 deficiency results in dysregulated erythropoiesis signaling and iron homeostasis in mouse development. *J. Biol. Chem.* **281,** 25703–25711
16. Gruber, M., Hu, C. J., Johnson, R. S., Brown, E. J., Keith, B., and Simon, M. C. (2007) Acute postnatal ablation of Hif-2α results in anemia. *Proc. Natl. Acad. Sci. U.S.A.* **104,** 2301–2306
17. Scortegagna, M., Ding, K., Zhang, Q., Oktay, Y., Bennett, M. J., Bennett, M., Shelton, J. M., Richardson, J. A., Moe, O., and Garcia, J. A. (2005) HIF-2α regulates murine hematopoietic development in an erythropoietin-dependent manner. *Blood* **105,** 3133–3140
18. Kapitsinou, P. P., Liu, Q., Unger, T. L., Rha, J., Davidoff, O., Keith, B., Epstein, J. A., Moores, S. L., Erickson-Miller, C. L., and Haase, V. H. (2010) Hepatic HIF-2 regulates erythropoietic responses to hypoxia in renal anemia. *Blood* **116,** 3039–3048
19. Percy, M. J., Furlow, P. W., Lucas, G. S., Li, X., Lappin, T. R., McMullin, M. F., and Lee, F. S. (2008) A gain-of-function mutation in the *HIF2A* gene in familial erythrocytosis. *N. Engl. J. Med.* **358,** 162–168
20. Percy, M. J., Beer, P. A., Campbell, G., Dekker, A. W., Green, A. R., Oscier, D., Rainey, M. G., van Wijk, R., Wood, M., Lappin, T. R., McMullin, M. F., and Lee, F. S. (2008) Novel exon 12 mutations in the *HIF2A* gene associated with erythrocytosis. *Blood* **111,** 5400–5402
21. Gale, D. P., Harten, S. K., Reid, C. D., Tuddenham, E. G., and Maxwell, P. H. (2008) Autosomal dominant erythrocytosis and pulmonary arterial hypertension associated with an activating HIF2α mutation. *Blood* **112,** 919–921
22. van Wijk, R., Sutherland, S., Van Wesel, A. C., Huizinga, E. G., Percy, M. J., Bierings, M., and Lee, F. S. (2010) Erythrocytosis associated with a novel missense mutation in the *HIF2A* gene. *Haematologica* **95,** 829–832
23. Martini, M., Teofili, L., Cenci, T., Giona, F., Torti, L., Rea, M., Foà, R., Leone, G., and Larocca, L. M. (2008) A novel heterozygous HIF2AM535I mutation reinforces the role of oxygen sensing pathway disturbances in the pathogenesis of familial erythrocytosis. *Haematologica* **93,** 1068–1071
24. Copeland, N. G., Jenkins, N. A., and Court, D. L. (2001) Recombineering. A powerful new tool for mouse functional genomics. *Nat. Rev. Genet.* **2,** 769–779
25. Liu, P., Jenkins, N. A., and Copeland, N. G. (2003) A highly efficient recombineering-based method for generating conditional knockout mutations. *Genome Res.* **13,** 476–484
26. Yagi, T., Ikawa, Y., Yoshida, K., Shigetani, Y., Takeda, N., Mabuchi, I., Yamamoto, T., and Aizawa, S. (1990) Homologous recombination at c-*fyn* locus of mouse embryonic stem cells with use of diphtheria toxin A-fragment gene in negative selection. *Proc. Natl. Acad. Sci. U.S.A.* **87,** 9918–9922
27. Laird, P. W., Zijderveld, A., Linders, K., Rudnicki, M. A., Jaenisch, R., and Berns, A. (1991) Simplified mammalian DNA isolation procedure. *Nucleic Acids Res.* **19,** 4293
28. Li, X., Sutherland, S., Takeda, K., Fong, G. H., and Lee, F. S. (2010) Integrity of the prolyl hydroxylase domain protein 2:erythropoietin pathway in aging mice. *Blood Cells Mol. Dis.* **45,** 9–19
29. Nakagawa, Y., Kishida, K., Kihara, S., Funahashi, T., and Shimomura, I. (2009) Adiponectin ameliorates hypoxia-induced pulmonary arterial remodeling. *Biochem. Biophys. Res. Commun.* **382,** 183–188
30. Lifshitz, L., Tabak, G., Gassmann, M., Mittelman, M., and Neumann, D. (2010) Macrophages as novel target cells for erythropoietin. *Haematologica* **95,** 1823–1831
31. Rankin, E. B., Rha, J., Selak, M. A., Unger, T. L., Keith, B., Liu, Q., and Haase, V. H. (2009) Hypoxia-inducible factor 2 regulates hepatic lipid metabolism. *Mol. Cell. Biol.* **29,** 4527–4538
32. Rankin, E. B., Rha, J., Unger, T. L., Wu, C. H., Shutt, H. P., Johnson, R. S., Simon, M. C., Keith, B., and Haase, V. H. (2008) Hypoxia-inducible factor-2 regulates vascular tumorigenesis in mice. *Oncogene* **27,** 5354–5358
33. Rankin, E. B., Tomaszewski, J. E., and Haase, V. H. (2006) Renal cyst development in mice with conditional inactivation of the von Hippel-Lindau tumor suppressor. *Cancer Res.* **66,** 2576–2583
34. Smith, T. G., Brooks, J. T., Balanos, G. M., Lappin, T. R., Layton, D. M., Leedham, D. L., Liu, C., Maxwell, P. H., McMullin, M. F., McNamara, C. J., Percy, M. J., Pugh, C. W., Ratcliffe, P. J., Talbot, N. P., Treacy, M., and Robbins, P. A. (2006) Mutation of von Hippel-Lindau tumour suppressor and human cardiopulmonary physiology. *PLoS Med.* **3,** e290
35. Hickey, M. M., Richardson, T., Wang, T., Mosqueira, M., Arguiri, E., Yu, H., Yu, Q. C., Solomides, C. C., Morrisey, E. E., Khurana, T. S., Christofidou-Solomidou, M., and Simon, M. C. (2010) The von Hippel-Lindau Chuvash mutation promotes pulmonary hypertension and fibrosis in mice. *J. Clin. Investig.* **120,** 827–839
36. Formenti, F., Beer, P. A., Croft, Q. P., Dorrington, K. L., Gale, D. P., Lappin, T. R., Lucas, G. S., Maher, E. R., Maxwell, P. H., McMullin, M. F., O'Connor, D. F., Percy, M. J., Pugh, C. W., Ratcliffe, P. J., Smith, T. G., Talbot, N. P., and Robbins, P. A. (2011) Cardiopulmonary function in two human disorders of the hypoxia-inducible factor (HIF) pathway. von Hippel-Lindau disease and HIF-2α gain-of-function mutation. *FASEB J.* **25,** 2001–2011
37. McLaughlin, V. V., Archer, S. L., Badesch, D. B., Barst, R. J., Farber, H. W., Lindner, J. R., Mathier, M. A., McGoon, M. D., Park, M. H., Rosenson, R. S., Rubin, L. J., Tapson, V. F., and Varga, J. (2009) ACCF/AHA 2009 expert consensus document on pulmonary hypertension a report of the American College of Cardiology Foundation Task Force on Expert Consensus Documents and the American Heart Association developed in collaboration with the American College of Chest Physicians; American Thoracic Society, Inc.; and the Pulmonary Hypertension Association. *J. Am. Coll. Cardiol.* **53,** 1573–1619
38. Archer, S. L., Weir, E. K., and Wilkins, M. R. (2010) Basic science of pulmonary arterial hypertension for clinicians. New concepts and experimental therapies. *Circulation* **121,** 2045–2066
39. Rabinovitch, M. (2008) Molecular pathogenesis of pulmonary arterial hypertension. *J. Clin. Investig.* **118,** 2372–2379
40. Teng, X., Li, D., Champion, H. C., and Johns, R. A. (2003) FIZZ1/RELMα, a novel hypoxia-induced mitogenic factor in lung with vasoconstrictive and angiogenic properties. *Circ. Res.* **92,** 1065–1067
41. Kwapiszewska, G., Wygrecka, M., Marsh, L. M., Schmitt, S., Trösser, R.,

Wilhelm, J., Helmus, K., Eul, B., Zakrzewicz, A., Ghofrani, H. A., Schermuly, R. T., Bohle, R. M., Grimminger, F., Seeger, W., Eickelberg, O., Fink, L., and Weissmann, N. (2008) Fhl-1, a new key protein in pulmonary hypertension. *Circulation* **118,** 1183–1194

42. Diebold, I., Kraicun, D., Bonello, S., and Görlach, A. (2008) The "PAI-1 paradox" in vascular remodeling. *Thromb. Haemost.* **100,** 984–991
43. Xu, W., Kaneko, F. T., Zheng, S., Comhair, S. A., Janocha, A. J., Goggans, T., Thunnissen, F. B., Farver, C., Hazen, S. L., Jennings, C., Dweik, R. A., Arroliga, A. C., and Erzurum, S. C. (2004) Increased arginase II and decreased NO synthesis in endothelial cells of patients with pulmonary arterial hypertension. *FASEB J.* **18,** 1746–1748
44. Nemenoff, R. A., Simpson, P. A., Furgeson, S. B., Kaplan-Albuquerque, N., Crossno, J., Garl, P. J., Cooper, J., and Weiser-Evans, M. C. (2008) Targeted deletion of PTEN in smooth muscle cells results in vascular remodeling and recruitment of progenitor cells through induction of stromal cell-derived factor-1α. *Circ. Res.* **102,** 1036–1045
45. Weissmann, N., Manz, D., Buchspies, D., Keller, S., Mehling, T., Voswinckel, R., Quanz, K., Ghofrani, H. A., Schermuly, R. T., Fink, L., Seeger, W., Gassmann, M., and Grimminger, F. (2005) Congenital erythropoietin over-expression causes "anti-pulmonary hypertensive" structural and functional changes in mice, both in normoxia and hypoxia. *Thromb. Haemost.* **94,** 630–638
46. Bushuev, V. I., Miasnikova, G. Y., Sergueeva, A. I., Polyakova, L. A., Okhotin, D., Gaskin, P. R., Debebe, Z., Nekhai, S., Castro, O. L., Prchal, J. T., and Gordeuk, V. R. (2006) Endothelin-1, vascular endothelial growth factor and systolic pulmonary artery pressure in patients with Chuvash polycythemia. *Haematologica* **91,** 744–749
47. Brusselmans, K., Compernolle, V., Tjwa, M., Wiesener, M. S., Maxwell, P. H., Collen, D., and Carmeliet, P. (2003) Heterozygous deficiency of hypoxia-inducible factor-2α protects mice against pulmonary hypertension and right ventricular dysfunction during prolonged hypoxia. *J. Clin. Invest.* **111,** 1519–1527
48. Furlow, P. W., Percy, M. J., Sutherland, S., Bierl, C., McMullin, M. F., Master, S. R., Lappin, T. R., and Lee, F. S. (2009) Erythrocytosis-associated HIF-2α mutations demonstrate a critical role for residues C-terminal to the hydroxylacceptor proline. *J. Biol. Chem.* **284,** 9050–9058
49. Percy, M. J., Chung, Y. J., Harrison, C., Mercieca, J., Hoffbrand, A. V., Dinardo, C. L., Santos, P. C., Fonseca, G. H., Gualandro, S. F., Pereira, A. C., Lappin, T. R., McMullin, M. F., and Lee, F. S. (2012) Two new mutations in the *HIF2A* gene associated with erythrocytosis. *Am. J. Hematol.* **87,** 439–442
50. Yamashita, T., Ohneda, O., Sakiyama, A., Iwata, F., Ohneda, K., and Fujii-Kuriyama, Y. (2008) The microenvironment for erythropoiesis is regulated by HIF-2α through VCAM-1 in endothelial cells. *Blood* **112,** 1482–1492
51. Gordeuk, V. R., Sergueeva, A. I., Miasnikova, G. Y., Okhotin, D., Voloshin, Y., Choyke, P. L., Butman, J. A., Jedlickova, K., Prchal, J. T., and Polyakova, L. A. (2004) Congenital disorder of oxygen sensing. Association of the homozygous Chuvash polycythemia VHL mutation with thrombosis and vascular abnormalities but not tumors. *Blood* **103,** 3924–3932
52. Kim, W. Y., Safran, M., Buckley, M. R., Ebert, B. L., Glickman, J., Bosenberg, M., Regan, M., and Kaelin, W. G., Jr. (2006) Failure to prolyl hydroxylate hypoxia-inducible factor α phenocopies VHL inactivation *in vivo*. *EMBO J.* **25,** 4650–4662